ASTROBIOLOGY
Volume 9, Number 9, 2009
© Mary Ann Liebert, Inc.
DOI: 10.1089/ast.2009.0345

# A Biosignature Suite from Cave Pool Precipitates, Cottonwood Cave, New Mexico

L.A. Melim,[1] R. Liescheidt,[1] D.E. Northup,[2] M.N. Spilde,[3] P.J. Boston,[4] and J.M. Queen[5]

## Abstract

Calcite cave pool precipitates often display a variety of potential biosignatures from the macroscopic to the submicroscopic. A fossil cave pool in Cottonwood Cave, New Mexico, exhibits older stalactites and stalagmites that are completely coated in brown, laminated calcitic crust that extends down as pool fingers and u-loops. The pool fingers and u-loops are mainly micrite to clotted micrite, some recrystallized to microspar, with some isopachous spar layers. Micrite, particularly clotted micrite, is usually interpreted by carbonate workers as microbial in origin. Scanning electron microscopy examination of etched pool fingers, u-loops, and the brown crust revealed abundant calcified microbial filaments and biofilm. Energy dispersive X-ray analysis showed that these features have excess carbon, above that found in pure calcite. Independent carbon analysis indicated that these same samples contain up to 0.2% organic carbon. Since pool fingers hang down but form underwater, we hypothesize they are biogenic with hanging microbial filaments or biofilm acting as nuclei for calcite precipitation. Because of the abundance of micrite and fossil filaments, we further hypothesize that these pendant features formed during a period of plentiful nutrients and active hydrological activity when the pool was literally dripping with microbial slime. Although each of these lines of evidence could be interpreted in other ways, their combined weight strongly suggests the cave pool precipitates in Cottonwood Cave are biogenic. These investigations can be used to help inform extraterrestrial life-detection studies. Key Words: Biosignatures—Biofilm—Microbial fossils—Life detection—Ca carbonate biofabrics. Astrobiology 9, 907–917.

## Introduction

Recent work has shown that caves are a remarkable repository of microbial life (Barton and Northup, 2007, and references therein). Caves provide an ideal environment for chemolithoautotrophic and heterotrophic growth of microbial communities that can contribute to both speleogenesis (Engel, 2007, and references therein) and later growth of speleothems (Forti, 2001; Melim *et al.*, 2001; Baskar *et al.*, 2005). While culturing and culture-independent (*i.e.*, molecular DNA) methods can elucidate the living cave community (Cacchio *et al.*, 2004; Barton and Northup, 2007), fossil systems are much more difficult to study (Barton *et al.*, 2001; Boston *et al.*, 2001; Jones, 2001; Barton and Northup, 2007; Engel, 2007). The key to documenting a fossil community lies in the occurrence of biosignatures: traces of life left behind long after the living community is gone. However, single biosignatures are often difficult to interpret, as various abiotic processes can mimic biotic ones (Jones, 2001). Therefore, we prefer to use a biosignature suite (Boston *et al.*, 2001), a collection of different but related chemical (*e.g.*, fatty acids or DNA), isotopic, and morphological biosignatures. An individual biosignature may be ambiguous, but a number of biosignatures, in concert, can provide strong evidence and contribute to documentation of the role of microbes in speleothem growth.

Speleothems that exhibit evidence of microbial life, such as filaments, hyphae, or webs of mineralized biofilm, are called biothems (Cunningham *et al.*, 1995). Although there are exceptions, most purported biothems are related to cave pools (Queen and Melim, 2006). Pool fingers, pendant speleothems that form underwater in cave pools, are one such type of biothem (Davis *et al.*, 1990; Hill and Forti, 1997; Melim *et al.*, 2001). Their pendant form has led several workers to suggest a microbial origin (Davis *et al.*, 1990; Melim *et al.*, 2001), given that strictly inorganic precipitation underwater should not produce forms that hang directly

[1]Geology Department, Western Illinois University, Macomb, Illinois.
[2]Biology Department and [3]Institute of Meteoritics, University of New Mexico, Albuquerque, New Mexico.
[4]National Cave and Karst Research Institute, c/o New Mexico Tech Earth & Environmental Science Department, Socorro, New Mexico.
[5]Guadalupe Mountain Institute, Carlsbad, New Mexico.

downward. In fact, abiotic pool spar (Hill and Forti, 1997) typically radiates in all directions equally as it coats the sides, bottoms, or even the ceilings of cave pools. Field morphology alone, however, is not definitive evidence for a biogenic origin. Here, we report on a location of pool fingers where a variety of biosignatures support the interpretation that these features are biothems.

The astrobiological value of structures like the pool fingers discussed here lies in the excellent preservation of biotextures and biofabrics that can be directly tied to prior biological activities. The more that such morphological, geochemical, and even biochemical traces can be tied to demonstrable activities of living organisms, the stronger becomes the circumstantial case that they are the result of biological activity in a rock and mineral environment. Excellent preservation has been seen in very ancient Earth materials (*cf.* Westall, 2008). Because of the antiquity of that material, however, the direct link to living examples is more challenging to make. Thus, it is important to work in preserved biotextural systems that are of more recent origin, where living analogues may also be uncovered and provide end points in time (Boston *et al.*, 2001). Such biosignatures and living analogues, and the means to detect them, are of potentially great utility as we explore the rocky surfaces of our neighboring planets and icy moons in search of indications of past life.

## Field Setting

Cottonwood Cave is located in the Guadalupe Ranger District of the Lincoln National Forest in southeastern New Mexico, USA (Fig. 1). The cave entrance is at 2040 m, over 300 m above the static water table (Hill, 1987; Polyak *et al.*, 1998). Due to the desert environment of southeastern New Mexico, the cave is mostly dry, though a number of former cave pools can be identified by the presence of a distinct waterline comprised of minerals that precipitated from the pool water.

No sunlight penetrates to that portion of the cave known as the Rattlesnake Room, which is located approximately 90 m below the surface. The Rattlesnake Room is roughly oval in shape and measures approximately 20 m by 7 m in length and width. The ceiling ranges up to 6 m in height. Polyak *et al.* (1998) dated the minimum age of Cottonwood Cave speleogenesis to 12.3 million years. After speleogenesis, the room drained, and over time flowstone, stalactites, stalagmites, and soda straws formed on the walls, ceiling, and floor (Fig. 2). A deep cave pool (up to 4 m) formed after this vadose stage, either because flowstone sealed the floor of the cave to create a perched pool or because of a rise in the water table. This pool is defined by a horizontal waterline composed of brown calcite crust (Fig. 2). This crust, and the features that extend from it, are the subject of this study. At this time, we have no age constraints on either the subaerial flowstone or the later subaqueous features.

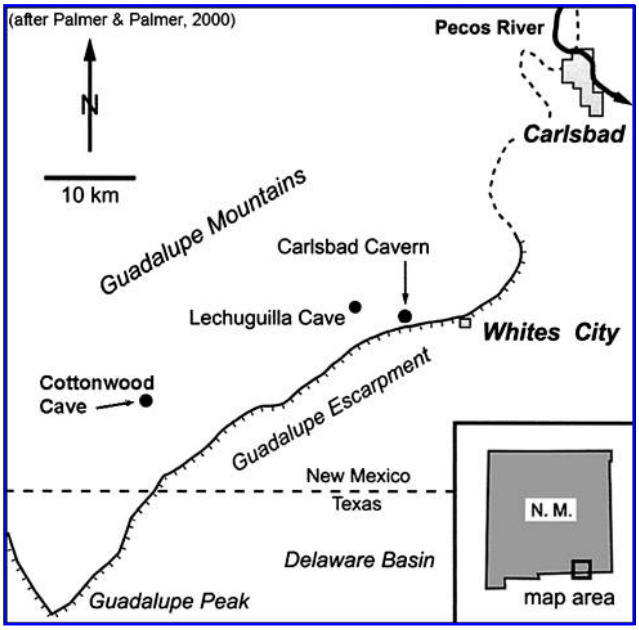


**FIG. 1.** Location map for Cottonwood Cave, located in southeastern New Mexico, USA. Also shown for reference are the well-known caves Lechuguilla Cave and Carlsbad Cavern. (Modified after Palmer and Palmer, 2000.)

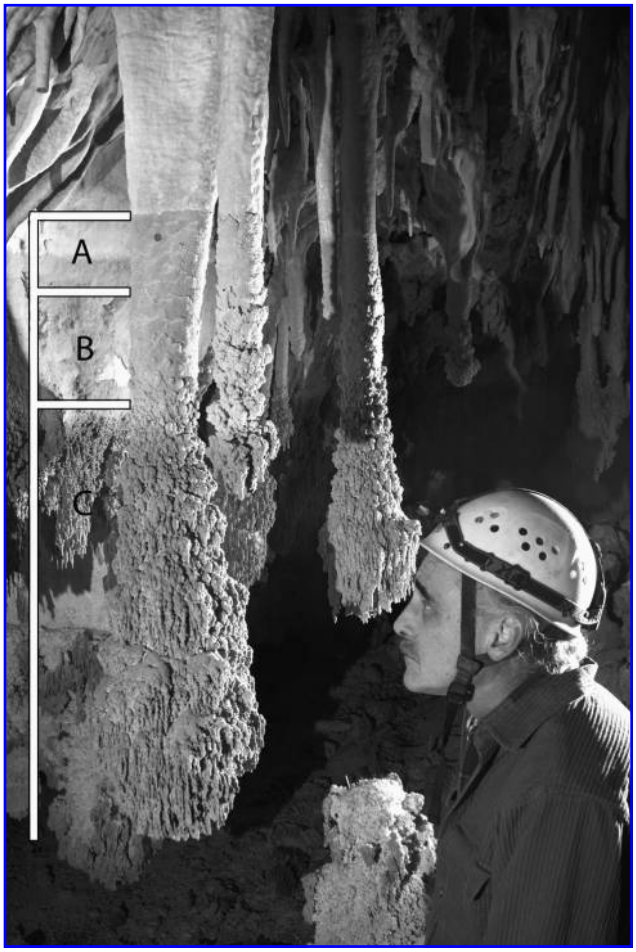


**FIG. 2.** The Rattlesnake Room brown crust coating an earlier stalactite. The brown crust starts smooth (**A**), then becomes knobby (**B**) before blossoming into many small pool fingers (**C**). Also note upper part of stalactite has altered to white chalky coating; this appears under the crust, so it started before the pool formed.

## Methods

To develop a complete context for the pool fingers, the Rattlesnake Room was described and photographed in detail. Scale drawings of all features were supplemented with photographs that included a scale. Five samples (limited under permit from the US Forest Service) of brown crust were collected from previously broken pieces where the context could be identified.

Thin sections were cut from the five samples and described and photographed at high magnification (to 40×) under a petrographic microscope. Uncovered thin sections were used to allow later scanning electron microscopy analysis; slides were coated in water to avoid contamination from immersion oil. Selected thin sections were examined for fossil microbes and relict biofilm in a JEOL 5800LV scanning electron microscope (SEM) at the University of New Mexico (UNM). Prior to imaging (and subsequent to petrography), the thin sections were lightly etched in 5% HCl solution for 10 seconds to remove the outermost carbonate and expose the microbial fossils. Our previous work has shown that this method emphasizes the fossil microbes, which, unlike the surrounding carbonate, do not dissolve during the etching process (Melim *et al.,* 2001). The samples were then coated with approximately 200 angstroms of gold-palladium alloy in an evaporative coater; the thin film of gold-palladium provides a conductive layer that is relatively free of artifacts and allows light element X-rays of carbon to pass with only moderate attenuation. The UNM SEM was equipped with an Oxford Isis 300 energy dispersive X-ray (EDX) analyzer. This modern EDX system utilizes a thin polymer-film window that allows for analysis of low-energy X-rays of light elements such as boron and carbon (Z.5). The SEM was operated at 15 kV accelerating voltage with a beam current of 10 pA, as measured in a Faraday cup. This gives a beam diameter of less than 50 nm. However, the electron beam samples a greater volume; and, with these operating conditions, the EDX analyzer provides a qualitative estimate of elements present in the upper 2–3 $\mu$m of a calcitic sample. In addition, a single chip was etched and examined on a JSM 6301FXV field-emission SEM at the University of Alberta. This sample was gold coated.

Detailed photomosaic images are used to correlate SEM observations to specific petrographic fabrics. By scratching a fiduciary mark on the surface of the thin section and then taking a detailed, scaled photomosaic with a digital camera, we were able to track our position with the XY position indicator on the SEM and then compare that position to the photomosaic by measuring distances, in millimeters, from the fiduciary mark. To quantify the distribution of fossil microbes and biofilm, each sample was scanned at the same magnification (4000×) while tracking the XY coordinates and counting the number of filaments, threads, or film in each field of view. By holding the magnification constant, we obtained a set area per field of view (25×30 $\mu$m). Using the horizontal distance traveled, we were able to calculate the area scanned and thus determine the number of features per square millimeter. The 4000× magnification was the minimum needed to spot filaments reliably, which resulted in a very time-consuming process; thus, relatively small areas were scanned, which ranged from 6000–60000 $\mu m^2$ ($\ll 1\,mm^2$) per petrographic fabric. The results, calculated as filaments/millimeter$^2$, provide relative abundances between different fabrics; but, due to the small sample size, we consider only large differences significant.

Percent nitrogen and percent carbon were determined by high-temperature combustion. The resulting gases were eluted on a gas chromatography column and detected by thermal conductivity and integrated to yield carbon and nitrogen content (Pella, 1990a, 1990b). Analyses were performed on a ThermoQuest CE Instruments NC2100 Elemental Analyzer, ThermoQuest Italia S.p.A., Rodano, Italy. The samples were dissolved in 6 *N* HCl acid prior to analysis to remove carbonate (Harris *et al.,* 2001).

Micrite is used herein to refer to carbonate grains that are less than 4 $\mu$m (after Folk, 1974), with no implication for the origin of these grains. We distinguish between dense micrite with a uniform dark color in transmitted light and clotted micrite with a spotty fabric of silt-sized micrite clumps surrounded by coarser spar (*sensu* Riding, 2000). *Filament* is a descriptive term for a curving stringlike feature much longer than it is wide. We use the term *thread* to indicate thin curving features that join or split; filaments do not split or join, though they may intertwine. To contrast, a *needle* is straight.

## Biosignature Suite

Our biosignature suite ranges from the macroscopic (field observations) to the microscopic (petrography) and submicroscopic (SEM and chemistry). Although each individual biosignature is not diagnostic, the combination provides strong support for a biological origin of the pool precipitates in the Rattlesnake Room of Cottonwood Cave. The suite is presented in the order observed, starting with the field data.

### *Field morphology*

Field relationships are critical to guiding the more detailed work that follows, even though they are not themselves diagnostic. This includes the setting of the Rattlesnake Room paleopool as well as the details of the pool precipitates.

The first speleothems that formed in the Rattlesnake Room were vadose features such as stalactites and stalagmites. These features are not currently active; and their surface, where exposed, has been etched and altered to a fine white powder (Figs. 3 and 4). Subsequent to these flowstone features, a pool formed. Moonmilk and then a brown crust coated all features in the pool. The horizontal waterline from this pool is clearly visible around the entire perimeter of the room as a sharp transition from white to gray flowstone to brown crust (Figs. 2 and 3). It is this brown crust that is the focus of this study.

The morphology of the brown crust varies with depth and position in the pool (*i.e.,* floor vs. submerged stalactites). The uppermost 5–10 cm (just beneath the pool line) is a smooth to slightly bumpy crust that thickens from zero at the waterline to a few millimeters 10 cm below the waterline (Fig. 2). From 10–40 cm below the waterline, protrusions extend out and upward 1–3 cm, giving an appearance of flower petals surrounding and extending out from the substrate (Fig. 2). At ~40 cm, the color of the brown crust darkens, giving the appearance of a second waterline (Fig. 2). However, the crust is continuous across this color change; a true second waterline would have shown a discontinuity within the crust. At

**FIG. 3.** Close-up of pool fingers growing from a submerged overhang. The crust does not coat the ceiling, but each small stalactite/soda straw has an expanded chandelier of pool fingers. This image is from 30–50 cm below the waterline seen in Fig. 2.

this depth, the crust becomes a mass of 2–5 mm diameter, 10–20 cm long pool fingers and u-loops that extend out and downward in an ever-widening cascade to form chandelier-like features that are 50 cm or more in diameter and extend downward 50–100 cm (Figs. 2, 3, and 4; the "Spanish moss" of Hill, 1987). Under submerged overhangs, small stalactites may act as nucleation points for chandeliers; a 1–10 cm stalactite often supports a 10–50 cm diameter chandelier (Fig. 3).

Stalagmites that sit under stalactites are coated with the same brown crust, which, unlike the case for stalactites, formed in both a downward and upward direction. The downward-growing crust is composed of connected pool fingers and u-loops similar to those that comprise the overhanging chandeliers, though the fingers are less defined. The upward-growing crust forms small, often branching, towers (Fig. 5). Where the submerged floor lacks overhanging stalactites, the brown crust forms small 1–3 cm knobs that, unlike the sharp crystalline surface of most pool spar, have a smooth surface (Fig. 6).

### *Petrographic fabric*

Petrography reveals the internal structure of the pool precipitates. This helps unravel the events in the cave pool that contributed to biological or abiological mineral precipitation. In addition, the petrographic fabrics can help explain the changes in field morphology with depth in the paleopool.

The brown crust is composed of complex layers of equant to dogtooth spar, dense micrite, clotted micrite, and yellow

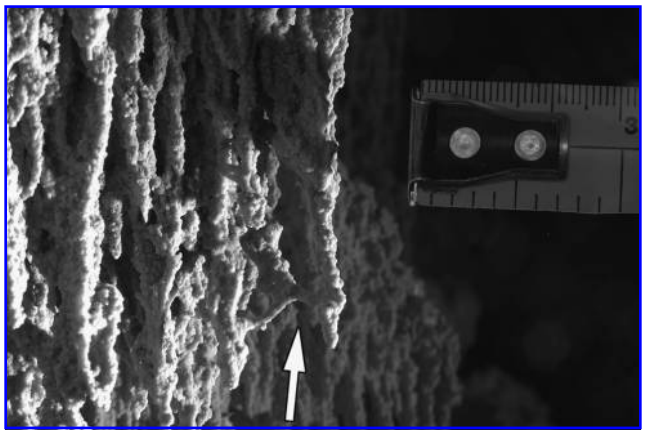

**FIG. 4.** Detail of pool fingers with u-loops connecting the tips (arrow).

**FIG. 5.** Detail of small tower built on top of a stalagmite and under a chandelier of pool fingers. Tower is approximately 10 cm tall.

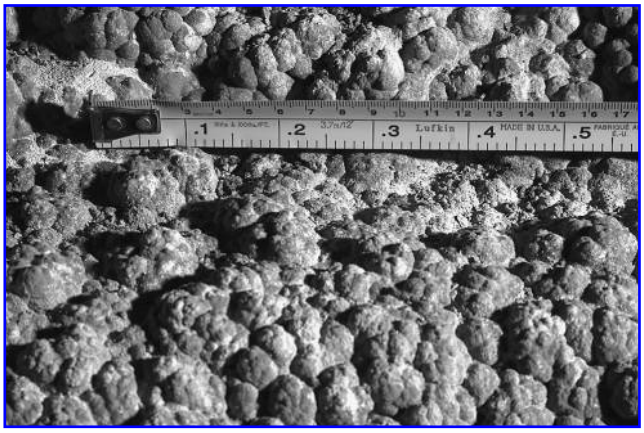


**FIG. 6.** Detail of brown crust on pool bottom in area with no pool fingers above. These brown knobs are similar to pool spar except they are smoother and composed of brown laminated crust, rather than the usually clear spar.

spar, all of which are composed of calcite (Fig. 7). EDX analysis showed no evidence of excess iron or magnesium. The initial coating is dense micrite followed by alternating layers of dogtooth spar and dense micrite. For the first 3–4 mm, both layers are mainly isopachous (equal thickness), though the micrite layers occasionally thicken by 0.1–0.2 mm into small clumps (Fig. 7A). Above about 4 mm, the smooth crust near the waterline stays isopachous, but lower knobby crust exhibits larger 1–2 mm clumps of clotted or peloidal micrite that form the cores of the knobs (Fig. 7A). Later spar and micrite layers then formed isopachous layers around these cores.

The spar layers are equant to dogtooth spar. Thicker layers have more elongate crystals, often with pale brown fibrous inclusions parallel to length. The outer surface of the crust is euhedral spar with slightly curved faces (Fig. 8A). Individual layers start with many equant crystals but then coalesce to larger, elongate through-going crystals. In some cases, the crystals extend from one spar layer through a micrite layer into the next spar layers. Where the micrite layers are thicker, the subsequent spar layers start over with many small crystals that then coalesce outward.

The equant to dogtooth spar is transparent when compared to the dark micrite layers. However, closer inspection reveals small dark inclusions and distinct curved filaments that extend through one or more crystals (Fig. 7B). The dark inclusions and filaments are also present in some micrite layers, but the dark, dense texture makes them hard to see. The inclusions are 5–10 $\mu$m in diameter, and the filaments are $\leq$1 $\mu$m in diameter and 50–200 $\mu$m in length. They may occur together, though most are not touching. Filaments occur alone, or several may intertwine (Fig. 7B).

When the brown crust extends downward as pool fingers, the layers are more irregular, and there is evidence for recrystallization (Fig. 7C, 7D). Dense micrite forms the core, and a mixture of micrite and yellow microspar (10–20 $\mu$m) comprise the greater part of each finger. The yellow microspar is probably a recrystallization of originally finer micrite, based on its equant form, irregular distribution within micrite areas, abundant patchy porosity, and the presence of dark residue between some crystals (Fig. 7D). Filaments and dark inclusions are common in one sample but absent in the other.

### *SEM observations*

Three distinct features of interest were found via scanning electron microscopy analysis: smooth filaments, reticulated filaments, and thin threads and films. Since the samples were etched, these features were not surface contaminants but were contained within the sample.

Scanning electron microscopy analysis revealed that both the smooth and reticulated filaments are similar in size to filaments observed optically, 0.5–1.0 $\mu$m in diameter and usually 1–10 $\mu$m (up to 100 $\mu$m) long (Fig. 8). Length, however, is an artifact of preservation, as the ends of these filaments are usually broken or buried in the calcite matrix.

Both types of filaments occur as either hollow or solid tubes. Smooth filaments, as the name implies, are simple tubes with no surface texture, whereas reticulated filaments have an open cross-hatched mesh similar to a honeycomb or fish net (Fig. 8E; Melim *et al.*, 2008). In addition to filaments, thin threads and films of carbon-rich material often bridge gaps and coat grains (Fig. 8D). These threads are often much smaller than the filaments (down to $<$0.1 $\mu$m). In addition, they branch and intertwine, and vary in thickness. Under the heat of the electron beam (15 Kv), the films sometimes shrank and cracked; filaments rarely did the same. Both smooth and reticulated filaments can occur with the threads and film, but they almost never occur together.

Filaments, threads, and films all showed elevated carbon content when analyzed by EDX (Fig. 8B, 8C, 8E, 8F). Since the area analyzed (2–3 $\mu$m) was always greater than the filament (1 $\mu$m), each analysis also included the underlying carbonate matrix. We estimated the excess carbon by comparing a spectrum of calcium carbonate to the spectra from the filaments, which was collected under the same conditions.

The UNM instrument results show a carbon peak for calcium carbonate that is one-half to two-thirds the height of the oxygen peak, and the oxygen peak is less than the calcium peak (Fig. 9). Nothdurft and Webb (2009) reported a similar relationship for other carbonate minerals. In some areas of our samples, clays were also present, based on morphology and the presence of silicon, aluminum, and magnesium; this resulted in an increase in the relative height of the oxygen peak (Fig. 8C). Therefore, if the carbon intensity is equal, or greater than, the oxygen peak, then excess carbon, above that in a carbonate, is present (Fig. 8C, 8F).

We compared the concentration of carbon-rich filaments and films in each petrographic fabric. For counting purposes, each filament counted as one, and each area of threads and film was counted as one (rather than trying to count individual threads, Table 1). Given the limited number of samples, small differences are probably not significant. Both micrite and spar areas contained significant numbers of filaments/film ($>$200 per mm$^2$; Table 1), many more than suggested by what was visible in thin section (generally $<$1 filament/mm$^2$). The one yellow microspar area that lacked any filaments in thin section was also devoid of filaments in the SEM. The greatest density came from a patch of clotted micrite in the center of a pool finger (1941 per mm$^2$; Fig. 7C), an area too opaque to see filaments in thin section. For

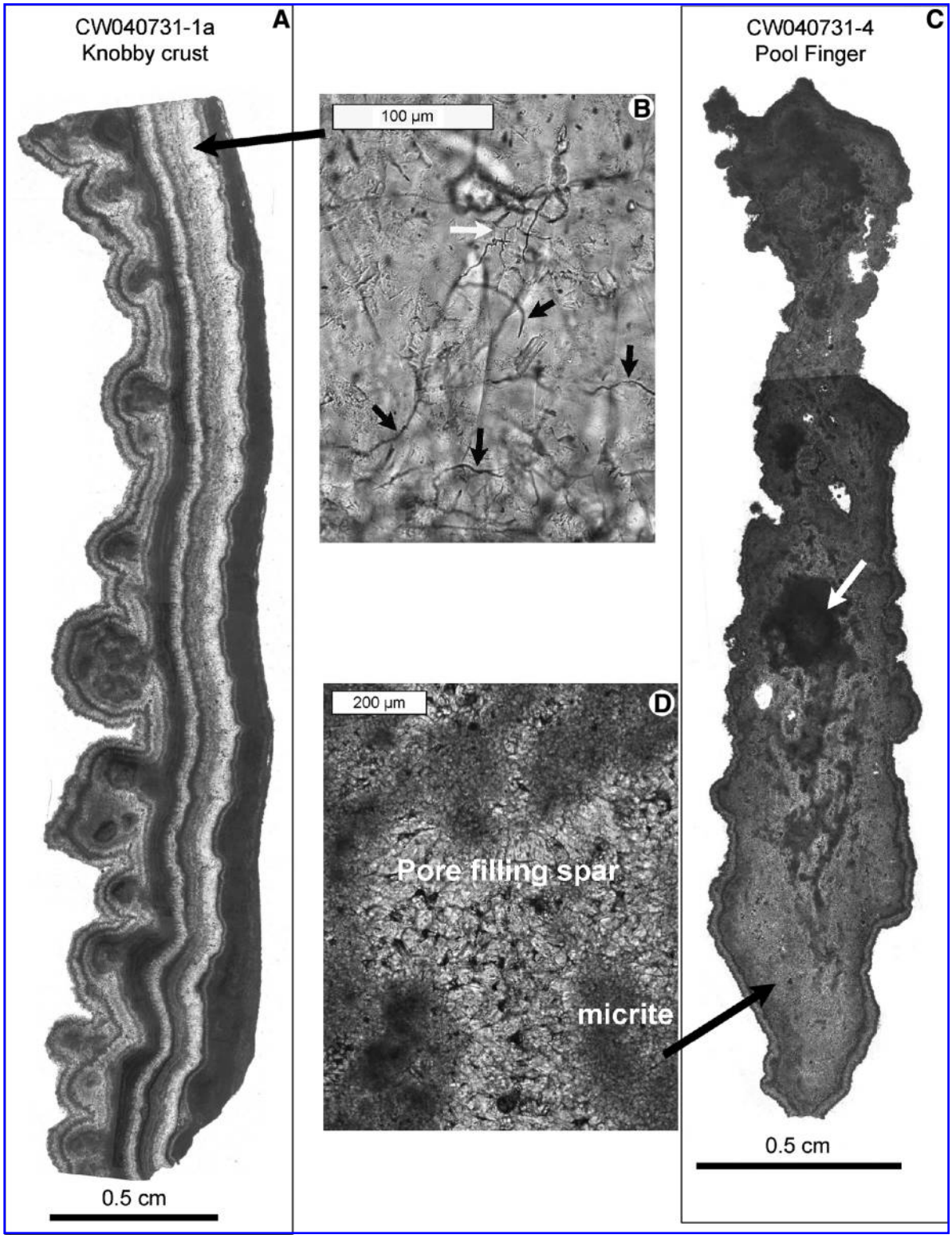


**FIG. 7.** Thin section photomicrographs of the brown crust. (**A**) Knobby crust 10–20 cm below the waterline composed of alternating micritic and spar layers. The knobs have clotted micrite cores; later layers go around these cores. Black arrow shows location of (B). (**B**) Detail of filaments found in spar layer. (**C**) Pool finger with micrite and clotted micrite core. Black arrow shows location of (D); white arrow shows location of greatest density of fossil microbes. (**D**) Detail of recrystallized spar in outer portion of pool finger.

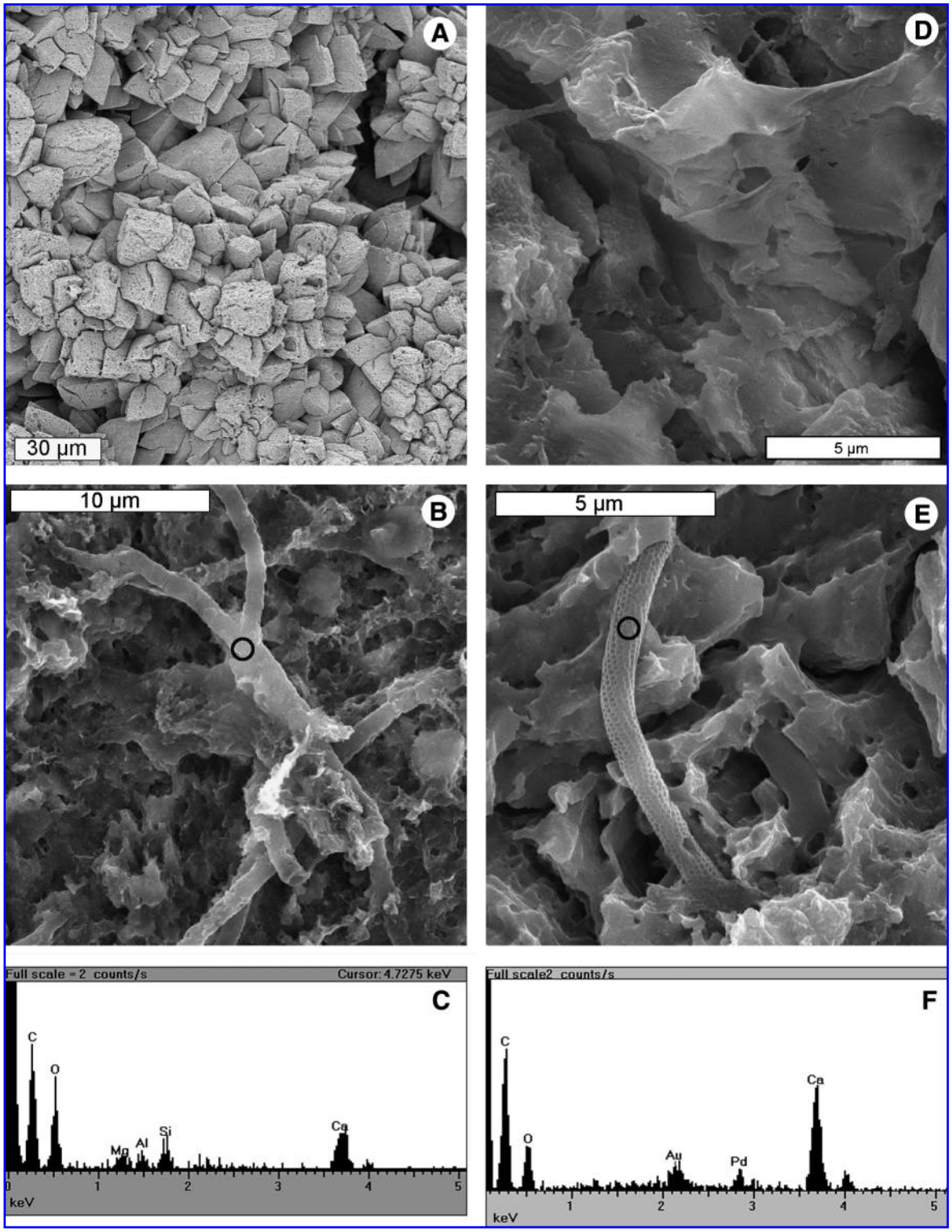


**FIG. 8.** SEM images of brown crust. (**A**) Surface texture showing euhedral crystals. Surface roughness is from etching the sample prior to viewing. (**B**) Smooth filaments in a matrix of calcite and clays (the crinkled-looking material). Note how the matrix partly covers the filaments, showing they were encased before etching. Circle shows location of EDX analysis in (C). (**C**) EDX of smooth filament in (B). Analysis shows Si, Al, Mg, and O from clays in matrix and Ca, O, and C from calcite in matrix. The C peak is much larger than the O peak even though the O peak is from both the carbonate and the clays; from the carbonate alone this peak should be much less than the Ca peak (Fig. 9). We interpret this excess C as indicating organic carbon in the filament. (**D**) Film and threads. Note the almost transparent nature of the film. (**E**) Reticulated filament. Note how the filament disappears into the matrix at the ends, showing it was encased in mineral before etching. Circle shows location of EDX analysis in (F). (**F**) EDX of reticulated filament in (D). Analysis shows Ca, O, and C from calcite in matrix with excess C, indicating organic carbon in the filament. The Au and Pd are from the coating.

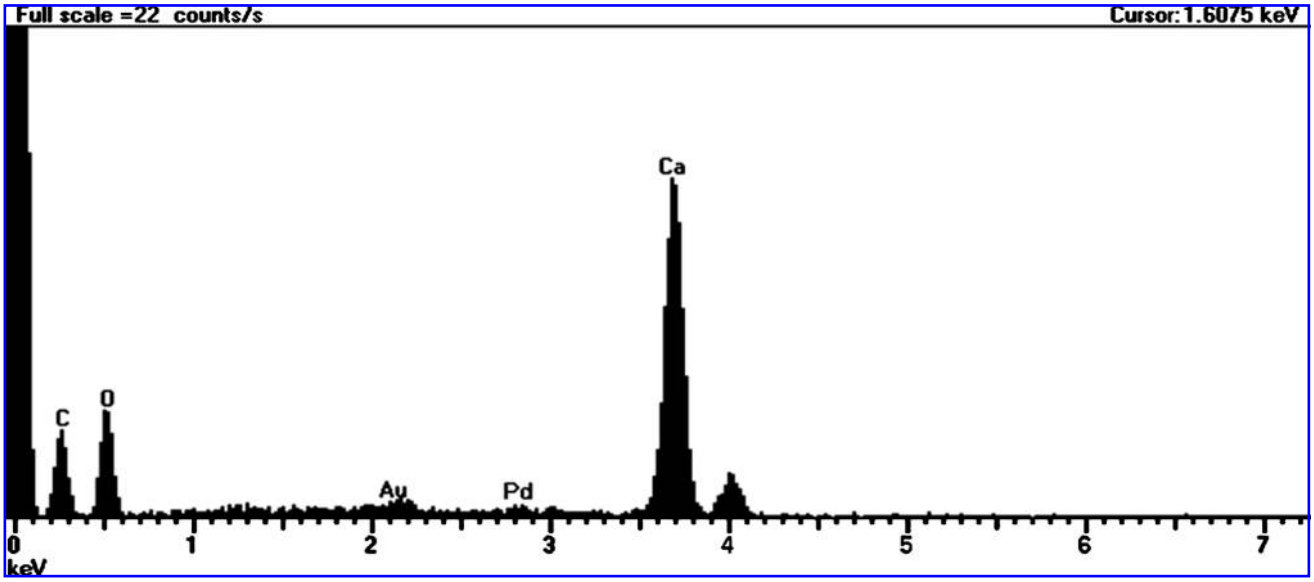


**FIG. 9.** EDX of calcite matrix. The carbon (C) peak is usually one-half to two-thirds the height of the oxygen (O) peak with the calcium (Ca) much larger than the oxygen. A higher carbon peak, therefore, indicates excess carbon above that in calcite (Fig. 8C, 8E). The Au and Pd are from the coating.

comparison, clear pool spar (generally agreed to be abiological precipitation) from Carlsbad Cavern contains no filaments or film (unpublished data).

### *Nitrogen and organic carbon content*

One pool finger sample was analyzed for organic carbon and nitrogen. It contained 0.1101% to 0.2241% organic carbon (average 0.1504%; $N = 4$) and 0.0026% to 0.0367% nitrogen (average 0.0154%). The detection limit of this method is 0.01% carbon and 0.001% nitrogen. In the oligotrophic cave environment, these values, while small, are significant.

## Discussion

### *Origin of filaments and other C-rich features*

We interpret the various filaments observed in thin section and SEM as being actual fossil microbes. This is based on their size, shape, and composition. The diameter of both smooth and reticulated filaments is consistently between 0.5 and 1.0 $\mu$m, which is the usual size for filamentous microbes. Since they are commonly hollow tubes in the SEM, this rules out a purely mineral origin, as minerals would be solid. The reticulated form, in particular, does not match any known minerals (Melim *et al.*, 2008). In addition, EDX analysis of filaments revealed a higher carbon content than expected for calcite alone (Figs. 8 and 9). Since the EDX analyzes the top 2–3 $\mu$m, each analysis included the underlying calcite matrix plus the filament. This indicates that the filaments include extra carbon, which in the cave context is presumably organic carbon.

The presence of organic carbon was independently confirmed by the organic carbon content, though there was no way to determine whether the measured organic carbon was composed of filaments. At this time, we do not know the exact form of the organic carbon, but a preserved organic filament would also explain why filaments resist the acid etching process that eats away the surrounding calcite ma-

Table 1. Number and Concentration of Carbon-Rich Filaments, Threads, and Film Found with the SEM

| *Sample name* | *Fabric scanned* | *Total area scanned microns*$^2$ | *# film areas* | *# filaments* | *Total #* | *Filaments/ mm*$^2$ |
|---|---|---|---|---|---|---|
| CW040731-1a | Micrite and clotted micrite knob | 6,160 | 1 | 1 | 2 | 325 |
| CW040731-1a | Spar layer | 64,878 | 9 | 16 | 25 | 385 |
| CW040731-1a | Micrite and clotted micrite | 50,138 | 4 | 26 | 30 | 598 |
| CW040731-1b | Micrite layer | 60,698 | 2 | 7 | 9 | 148 |
| CW040731-1b | Spar layer | 41,118 | 5 | 3 | 8 | 195 |
| CW040731-1b | Micrite layer | 19,778 | 6 | 2 | 8 | 404 |
| CW040731-2b | Micrite layer | 25,280 | 17 | 0 | 17 | 672 |
| CW040731-2b | Yellow microspar | 25,280 | 0 | 0 | 0 | 0 |
| CW040731-2b | Micrite core | 24,530 | 6 | 1 | 7 | 285 |
| CW040731-4 | Microspar and clotted micrite | 14,938 | 1 | 28 | 29 | 1,941 |
| CW040731-4 | Micrite core | 32,296 | 0 | 17 | 17 | 526 |

Individual smooth and reticulated filaments count as one filament; each patch of film/threads counts as one film area even though they are much larger than individual filaments. Note: the area scanned in each case is $<1\,mm^2$ ($1\,mm^2 = 1{,}000{,}000\,\mu m^2$).

trix. We speculate that the organic matter is preserved by being entombed by the growing calcite.

The threads and films extend down to sizes too small for fossil microbes (0.1 $\mu$m). However, they have the same carbon-rich composition and are often associated with filaments. We interpret these as fossil biofilm based on their similarity to known biofilms and their composition. The biofilms often shrink under an SEM beam, perhaps as the heat drives off water. While suggestive, this property alone is not definitive, as some clay minerals respond in a similar manner and are also fibrous. However, clay minerals would contain silicon and other cations, not the observed carbon.

### *Origin of the pendant pool fingers*

It is easy to understand why stalactites and soda straws grow downward; they form from water dripping into caves under the influence of gravity. It is less obvious how a pendant feature can form underwater, particularly in pools with evidence of a single waterline, which indicates a relatively constant water level. Gonzalez *et al.* (1992) hypothesized that "elongate crystals" under overhangs develop as a result of varying water level with the tips of the crystals following the rising and falling pool level. However, this model fails to explain two important characteristics of pool fingers: (1) even though they often taper, all fingers in a given pool are similar in size regardless of position (depth) in the pool (Figs. 2 and 3; Melim *et al.*, 2001) and (2) pools with pool fingers rarely show more than one waterline. If the pool fingers precipitated following a variable water level, then the fingers should vary in diameter depending on how long each part was submerged, and there should be independent evidence of the varying water levels. In the case of Cottonwood Cave, there is a single waterline, and all pool fingers are 2–5 mm in diameter and taper downward only slightly, regardless of depth below waterline (0.4–2 m; Figs. 2 and 3).

We prefer the alternative hypothesis that pool fingers form by encrusting microbial filaments or biofilm strands, physical features that would hang under the influence of gravity even underwater (Davis *et al.*, 1990; Melim *et al.*, 2001). This model better explains the observed form of pool fingers. Individual fingers nucleated on individual filaments or strands of biofilm; additional growth could be either biologically induced or abiologically precipitated on an organically derived core. The occurrence of the same 2–5 mm wide pool fingers over nearly 2 m of depth suggests one pool finger–forming event throughout the pool, related to the single observed pool level.

### *Origin of the brown crust and towers*

On the pool bottom, the brown crust is usually composed of simple knobs (Fig. 6) except underneath the pool fingers, where complex towers are built (Fig. 5). This suggests that the overhanging pool fingers were dripping biofilm that built up the underlying towers. However, the entire pool is coated in the brown crust, which suggests that microbes were living on all substrates and coating them in biofilm. Only where stalactites or an overhang provided a starting point were pool fingers formed, and this allowed formation of the underlying towers.

### *Origin of petrographic fabrics*

The petrographic fabrics also suggest microbial involvement. Micritic fabric can form either from the action of microbes (Chafetz, 1986; Riding, 2000; Cañaveras *et al.*, 2001; Jones, 2001) or by trapping of fine detrital grains (Cañaveras *et al.*, 2001; Jones, 2001). In the context of a cave pool, significant detrital micrite is unlikely but cannot be ruled out. In addition, clotted or peloidal micrite is a strong indicator of nucleation around microbial colonies (Chafetz, 1986; Chafetz and Buczynski, 1992; Riding, 2000).

The first layer in all samples is micrite, but the best-developed clotted micrite fabric occurs as the cores of small knobs protruding out from the crust 10–40 cm below the waterline (Fig. 7A). More-opaque dense micrite occurs as the core of individual fingers at deeper levels. This supports the hypothesis that microbes or biofilm caused initiation of pool finger growth. The alternation of micrite and spar layers indicates alternating pool conditions that were more conducive to forming micrite layers (more favorable for microbes) or more conducive to spar layer formation (less favorable for microbes or more favorable for abiotic mineral growth). Isopachous spar is a common feature in cave pools and can usually be attributed to precipitation by either $CO_2$ degassing or evaporation (Hill and Forti, 1997). However, based on the filaments present in the spar layers, microbes were always present on the surface (Table 1). Perhaps periodic influxes of nutrients led to episodes of more active growth, which, once the nutrients were consumed, were followed by periods of abiological precipitation. The micrite layers often contain clays (identified by Si, Al, and Mg with EDX; Fig. 8B, 8C), which suggests an associated influx of surface waters.

The presence of abundant fossil filaments and biofilm identified in transmitted light and SEM testify to an active microbial community during the formation of the pool fingers. If the micritic layers formed during periods of greater microbial growth, then a greater number of fossils would be expected in those layers. However, fossil microbes were found in both spar and micrite layers, generally in similar abundances (Table 1). This is contrary to our observations in other speleothems, where calcite spar rarely contains fossils (unpublished data), and suggests an active community even during lower nutrient periods. The calcite spar forms isopachous layers, which is expected for abiological growth into water. The knobs and fingers cored by clotted micrite are not isopachous. Rather, they either stick out or hang down (Figs. 2 and 7), indicating a different behavior from the isopachous spar, which we interpret as biologically induced precipitation. The knobs formed near the top of the pool, where microbial colonies were not large enough to create pendant features. We envision that, at the same time the knobs were forming, the microbial colonies deeper in the pool were large enough to produce the pendant pool fingers. This difference suggests that biofilm streamers, more than individual filaments, make up the core of these pool fingers. The presence of the towers beneath pool fingers, which were likely built up by drips of biofilm from above, also suggests that large amounts of biofilm were present when the pool was active.

## Implications

Conclusively determining a biological origin for any mineral structure is difficult, as many biological processes

mimic geological processes (Jones, 2001). Any single line of evidence is suspect, but a biosignature suite can strengthen a biological interpretation. In this case, the combination of field, petrographic, and SEM scale observations all point to a biological origin for the brown crust and pool fingers in the Rattlesnake Room of Cottonwood Cave. The total organic carbon and nitrogen data confirm the presence of organic matter and further strengthen the interpretation.

Caves, subsurface fissures, microcracks, and pore spaces between mineral grains all provide habitats that protect microorganisms from harmful surface conditions, which include weather, desiccation, temperature fluctuations, ultraviolet radiation, and grazing by higher organisms. In these protected habitats, microbes carry out their metabolic activities and often become lithified in place with subsequent extensive *in situ* preservation. The exquisite preservation of delicate biofilm, filaments, and cellular components in the calcite structures examined in this study demonstrates that ultrastructural features can survive long past the biologically active era of the environment. As a result, the subsurface on Earth offers one of the best environments in which to search for living, recently alive, and long-dead microbial life-forms, and the characteristic biosignatures they leave behind (Boston *et al.,* 1999; Boston, 2000). Thus, environments such as carbonate pools where biothems have been created and preserved offer unique opportunities to perfect our techniques for life-detection on Earth and beyond.

Lessons learned in these Earth environments, for example, can be applied to detecting life in the subsurface of Mars and other planets. On Mars, where surface conditions are particularly hostile, subsurface preserved materials would be protected against strong fluxes of short-wavelength ultraviolet radiation, ionizing radiation, and the global dust storms for which Mars is famous. The subsurface of Mars may reveal some of the only clues to life through preserved biosignatures (Boston *et al.,* 1992).

## Conclusions

A large paleopool in the Rattlesnake Room of Cottonwood Cave, New Mexico, is coated in a brown crust containing pool fingers that formed in association with an active microbial community based on the following biosignatures:

(1) *Pendant morphology:* The brown crust is a uniform coating on vertical walls but is knobby and pendant (pool fingers) when coating preexisting stalactites or overhangs. We conclude that the pendants formed by precipitation around filaments, biofilm streamers, or both. The tower features beneath the pool fingers form by drips of biofilm falling off the pool fingers.

(2) *Micrite to clotted micrite:* The core of knobs and fingers is composed of micrite and clotted micrite, which supports an interpretation of a microbial origin. The rest of the crust is laminated, isopachous micrite and calcite spar, more clotted micrite, or recrystallized calcite. We suggest that the micritic components formed because of an active microbial community, while the spar layers formed from an abiological process, likely due to degassing of $CO_2$ or evaporation.

(3) *Fossil filaments and biofilm:* Micrite, clotted micrite, and spar layers all contain fossil filaments, both smooth and reticulate varieties, along with fossil biofilm. EDX analyses showed that these fossils contain excess carbon, which indicates an organic composition. Organic carbon of up to 0.2% has been independently confirmed by acid dissolution and carbon analysis.

Each of these biosignatures is not sufficient alone to support an interpretation that the brown crust and pool fingers are biothems (*i.e.,* that they formed because of the microbial community). The combination of these biosignatures, however, provides strong support for a biogenic origin. The use of such a suite of characteristics (even though most are morphological) can provide enhanced confidence in a biological interpretation of such materials and has great significance for future interpretation of similar extraterrestrial samples.

## Acknowledgments

This material is based upon work supported by the National Science Foundation under Grants No. 0719710, 0719507, and 0719669. Additional funding was provided by a Western Illinois University College of Arts and Sciences Undergraduate Research and Creative Activity Grant to R. Liescheidt and a WIU University Research Council Grant to L. Melim.

We thank the US Forest Service for permission to sample in Cottonwood Cave. In addition, special thanks are owed to USFS employees Deanna Younger and Kevin Glover. Neil Shannon and Susan Herpin assisted in the field work. Many thanks to George Braybrook who took the SEM images at the University of Alberta. Special thanks to Kenneth Ingham who took many great photographs of our sampling sites and pool precipitates in the field.

## Author Disclosure Statement

No competing financial interests exist.

## Abbreviations

EDX, energy dispersive X-ray; SEM, scanning electron microscope; UNM, University of New Mexico.

## References

Barton, H.A. and Northup, D.E. (2007) Geomicrobiology in cave environments: past, current and future perspectives. *Journal of Cave and Karst Studies* 69:163–178.

Barton, H.A., Spear, J.R., and Pace, N.R. (2001) Microbial life in the underworld: biogenicity in secondary mineral formations. *Geomicrobiol. J.* 18:359–368.

Baskar, S., Baskar, R., Mauclaire, L., and McKenzie, J.A. (2005) Role of microbial community in stalactite formation, Sahastradhara caves, Dehradun, India. *Current Science* 88:1305–1308.

Boston, P.J. (2000) Life below and life "Out There." *Geotimes* 45:14–17.

Boston, P.J., Ivanov, M.V., and McKay, C.P. (1992) On the possibility of chemosynthetic ecosystems in subsurface habitats on Mars. *Icarus* 95:300–308.

Boston, P.J., Kleina, L.G., Soroka, D.S., Lavoie, K.H., Northup, D.E., Spilde, M.N., and Hose, L.D. (1999) Cave microbes: microbial mats lining hydrogen sulfide springs [abstract 36]. In *Abstracts and Programs from the 4th International Symposium on Subsurface Microbiology,* Vail, Colorado.

Boston, P.J., Spilde, M.N., Northup, D.E., Melim, L.A., Soroka, D.A., Kleina, L.G., Lavoie, K.H., Hose, L.D., Mallory, L.M., Dahm, C.N., Crossey, L.J., and Scheble, R.T. (2001) Cave biosignature suites: microbes, minerals and Mars. *Astrobiology* 1:25–55.

Cacchio, P., Contento, R., Ercole, C., Cappuccio, G., Martinez, M.P., and Lepidi, A. (2004) Involvement of microorganisms in the formation of carbonate speleothems in the Cervo Cave (L'Aquila-Italy). *Geomicrobiol. J.* 21:497–509.

Cañaveras, J.C., Sanchez-Moral, S., Soler, V., and Saiz-Jimenez, C. (2001) Microorganisms and microbially induced fabrics in cave walls. *Geomicrobiol. J.* 18:223–240.

Chafetz, H.S. (1986) Marine peloids: a product of bacterially induced precipitation of calcite. *J. Sediment. Petrol.* 56:812–817.

Chafetz, H.S. and Buczynski, C. (1992) Bacterially induced lithification of microbial mats. *Palaios* 7:277–293.

Cunningham, K.I., Northup, D.E., Pollastro, R.M., Wright, W.G., and LaRock, E.J. (1995) Bacteria, fungi and biokarst in Lechuguilla Cave, Carlsbad Caverns National Park, New Mexico. *Environ. Geol.* 25:2–8.

Davis, D.G., Palmer, M.V., and Palmer, A.N. (1990) Extraordinary subaqueous speleothems in Lechuguilla Cave, New Mexico. *Journal of Cave and Karst Studies* 52:70–86.

Engel, A.S. (2007) Observations on the Biodiverstiy of Sulfidic Karst Habitats. *Journal of Cave and Karst Studies* 69:187–206.

Folk, R.L. (1974) The natural history of crystalline calcium carbonate: effect of magnesium content and salinity. *J. Sediment. Petrol.* 44:141–153.

Forti, P. (2001) Biogenic speleothems: an overview. *Int. J. Speleol.* 30:39–56.

Gonzalez, L.A., Carpenter, S.J., and Lohmann, K.C. (1992) Inorganic calcite morphology: roles of fluid chemistry and fluid flow. *Journal of Sedimentary Research* 62:382–399.

Harris, D., Horwath, W.R., and Van Kessel, C. (2001) Acid fumigation of soils to remove carbonates prior to total organic carbon or carbon-13 isotopic analysis. *Soil Sci. Soc. Am. J.* 65:1853–1856.

Hill, C.A. (1987) *Geology of Carlsbad Cavern and Other Caves in the Guadalupe Mountains, New Mexico and Texas,* New Mexico Bureau of Mines and Mineral Resources, Socorro, NM.

Hill, C.A. and Forti, P. (1997) *Cave Minerals of the World,* 2nd ed., National Speleological Society, Huntsville, AL.

Jones, B. (2001) Microbial activity in caves—a geological perspective. *Geomicrobiol. J.* 18:345–358.

Melim, L.A., Shinglman, K.M., Boston, P.J., Northup, D.E., Spilde, M.N., and Queen, J.M. (2001) Evidence of microbial involvement in pool finger precipitation, Hidden Cave, New Mexico. *Geomicrobiol. J.* 18:311–330.

Melim, L.A., Northup, D.E., Spilde, M.N., Jones, B., Boston, P.J., and Bixby, R.J. (2008) Reticulated filaments in cave pool speleothems: microbe or mineral? *Journal of Cave and Karst Studies* 70:135–141.

Nothdurft, L.D. and Webb, G.E. (2009) Earliest diagenesis in scleractinian coral skeletons: implications for palaeoclimate-sensitive geochemical archives. *Facies* 55:161–201.

Palmer, A.N. and Palmer, M.V. (2000) Hydrochemical interpretation of cave patterns in the Guadalupe Mountains, New Mexico. *Journal of Cave and Karst Studies* 62:91–108.

Pella, E. (1990a) Elemental organic analysis. Part 1. Historical developments. *Am. Lab.* 22–3:116–115.

Pella, E. (1990b) Elemental organic analysis. Part 2. State of the Art. *Am. Lab.* 22–12:28–32.

Polyak, V.J., McIntosh, W.C., Güven, N., and Provencio, P. (1998) Age and origin of Carlsbad Cavern and related caves from $^{40}Ar/^{39}Ar$ of alunite. *Science* 279:1919–1922.

Queen, J.M. and Melim, L.A. (2006) Biothems: biologically influenced speleothems in caves of the Guadalupe Mountains, New Mexico, USA. In *Caves and Karst of Southeastern New Mexico,* New Mexico Geological Society Guidebook, 57th Field Conference, edited by W. Raatz, L. Land, and P. J. Boston, New Mexico Geological Society, Socorro, NM, pp 167–174.

Riding, R. (2000) Microbial carbonates: the geologic record of calcified bacterial-algal mats and biofilms. *Sedimentology* 47:179–214.

Westall, F. (2008) Morphological biosignatures in early terrestrial and extraterrestrial materials. *Space Sci. Rev.* 135:95–114.

Address correspondence to:
*Dr. L.A. Melim*
*Geology Department*
*Western Illinois University*
*1 University Circle*
*Macomb, IL 61455*

*E-mail:* LA-Melim@wiu.edu